Synchrony of trend shifts in Sahel boreal summer rainfall and global oceanic evaporation, 1950–2012

A. Diawara[1], Y. Tachibana[1], K. Oshima[2], H. Nishikawa[1] and Y. Ando[1]

[1]{Weather and Climate Dynamics Division, Mie University, Tsu, Japan}

[2]{Institute of Arctic Climate and Environment Research, Japan Agency for Marine-Earth Science and Technology, Yokosuka, Japan}

Correspondence to: Yoshihiro Tachibana (tachi@bio.mie-u.ac.jp)

Abstract

Between 1950 and 2012, boreal summer (rainy season) rainfall in the Sahel changed from a multi-decadal decreasing trend to an increasing trend (positive trend shift) in the mid-1980s. We found that this trend shift was synchronous with similar trend shifts in global oceanic evaporation and in land precipitation in all continents except the Americas. The trend shift in oceanic evaporation occurred mainly in the southern hemisphere (SH) and the subtropical oceans of the northern hemisphere (NH). Because increased oceanic evaporation strengthens the atmospheric moisture transport toward land areas, the synchrony of oceanic evaporation and land precipitation is reasonable. Surface scalar winds over the SH oceans also displayed a positive trend shift. Sea surface temperature (SST) displayed a trend shift in the mid-1980s that was negative (increasing, then decreasing) in the SH and positive in the NH. Although SST had opposite trend shifts in both hemispheres, the trend shift in evaporation was positive in both hemispheres. We infer that because strong winds promote evaporative cooling, the trend shift in SH winds strengthened the trend shifts of both SST and evaporation in the SH. Because high SST promotes evaporation, the trend shift in NH SST strengthened the NH trend shift in evaporation. Thus differing oceanic roles in the SH and NH generated the positive trend shift in evaporation; however, the details of moisture transport toward the Sahel are still unclear or perhaps there is no single determining influence.

1 Introduction

For the past sixty years, the West African Sahel region, located between 10°N – 20°N longitude, has been one of the most important research areas for studying climatic variability due to its fragile climate conditions. While there are many well-documented analyses of the Sahel's drought conditions since the early 1970s (e.g., Hulme, 1992, Christensen et al., 2007, Baines and Folland, 2007), there is no general explanation on the source of the drought. Several studies have also shown that the Indian Ocean, the North and South Atlantic Ocean, and the southern hemisphere (SH) oceans and the Mediterranean Sea have, alone or together, some kind of remote influence on the distribution of Sahel rainfall (Palmer, 1986; Giannini et al., 2003; Wolter, 1989; Janicot et al., 1996; Rowell, 2003; Hagos and Cook, 2008; Diatta and Fink, 2014). Studies and evaluations of the Sahel monsoon are crucial to determine previous precipitation variations, provide climate projections, and offer a scientific response to the decrease in rainfall over the majority of the region (Dai et al., 2001, Omotosho et al., 2008); however, the exact linkage between the multi-decadal variations of the Sahel rainfall and the global ocean remain unclear. Sahel rainfall is correlated with remote SST, which suggests that global-scale ocean evaporation processes are potentially important for the historical land surface rainfall variability. Our initial analysis suggested that the global hydrological cycle is comprised of evaporation from some part of the ocean surface and the transport of water vapor over the African continent. Therefore, it is reasonable that moisture transport from different parts of the world ocean may, either alone or in combination, affect African precipitation in general and that of the Sahel in particular.

Some of the earliest works related to nearby sea surface temperatures (SSTs) have shown that precipitation time's series have significantly changed over the last sixty years (Lough, 1986; Bader and Latif, 2003; Chung and Ramanathan, 2006). Other studies related to remote SST point out that the precipitation time's series has considerably changed over that the past sixty years as well (Folland et al., 1986; Janicot et al., 1996; Rowell, 2003; Fontaine et al., 2011; Munemoto and Tachibana, 2012; Diatta and Fink, 2014). The potential long-term causes and effects of SST variability are important inputs for the thermo-dynamical process of Sahel rainfall (Folland et al. 1986; Giannini et al. 2003; Tippett & Giannini 2006; Lu and Delworth 2005; Hoerling et al. 2006). Although long-term climate trends are commonly related to the state of the ocean, the radiative forcing by changing levels of greenhouse gas and/or aerosols have been considered

responsible for the changes of climate in the global ocean and on each continent except Antarctica (Stott et al., 2010). Yet, the increased trend of the greenhouse gas has not been linked to the trend shift of the Sahel rainfall. Delworth et al. (1993) defined the thermal impacts of the North Atlantic thermohaline overturning flow at multi-decadal scales. Zhang and Delworth (2006) referred to the subsequent SST pattern as the Atlantic Multi-decadal Oscillation. Pomposi et al. (2015) examined the role of global SST anomalies and their effects on monsoon variability in the Sahel region and found that "much of the internal variability of the global monsoon system" is generated by SST variances and their outcome on the atmospheric teleconnections, linking oceanic variations to land-based rainfall. Munemoto and Tachibana (2012) demonstrated that the contrast between North and South SST also corresponds to the more recent pattern of Sahel rainfall; in the mid-1980s, the phenomenon shifted from a decreasing trend to an increasing trend. These various studies underscore the lack of a single mechanism determining the relationship between the shift of the Sahel rainfall and the shift of oceanic evaporation. Folland et al. (1986) were among the first to historically establish a relationship between Sahel rainfall and (SH) SST on multi-decadal time scales; this relationship has demonstrated that when the SH SST is higher (lower) than normal, the Sahel is drier (wetter) than normal (Folland et al., 1986). Bader and Latif (2003) considered the warming trend in the Indian Ocean to have "a crucial role for the [forty-year] drying trend over the West Sahel." As a consequence, Indian Ocean warming may have contributed to the strengthening of the North Atlantic Oscillation during these last two decades. In addition, their experiments highlight the influence of the tropical Pacific over the eastern Sahel, whereas the tropical Atlantic influences rainfall only over the Atlantic itself and along the western Sahel.

For this study, we analyzed global evaporation datasets for the second half of the 20th century in order to determine whether the previously established linkages between remote SST and Sahel rainfall are the result of remote linkages between Sahel rainfall and oceanic evaporation. We also investigated the underlying trends in wind stress and SST that may explain changes in evaporation. Given the region's exposure to natural variability, favoring severe drought with unexplained sequence variations, this study will deliver a skillful multi-decadal climate forecast for the Sahel.

2 Data and Methods

For the precipitation, we used 3 different monthly datasets: from 1949 to 2014, the National Oceanic and Atmospheric Administration (NOAA) Precipitation Reconstruction over Land (PREC/L) database (Chen et al., 2002) with a spatial resolution of 1.0 degree in latitude and longitude; the Global Precipitation Climatology Centre (GPCC) data (Schneider et al. 2011), 2.5x2.5, from 1949 to 2013; and the University of Delaware UDel_AirT_Precip data provided by the NOAA/OAR/ESRL PSD, Boulder, Colorado, USA, from their Web site at http://www.esrl.noaa.gov/psd/, resolution of 0.5x0.5 and from 1949 to 2013. For SST, we used monthly data from 1953 to 2012 in the NOAA Extended Reconstructed SST Version 3 (NOAA ERSST V3) dataset, which is constructed from SST data in the International Comprehensive Ocean-Atmosphere Data Set (ICOADS) (Smith et al., 2008; Xue et al., 2003). Monthly 10-m scalar wind speed data from 1950 to 2011 came from Wave and Anemometer-based Sea Surface Wind (WASWind) version 1.0.1 (Tokinaga and Xie, 2011), derived from ship observations in ICOADS and presented at a resolution of 4 × 4 degrees. Specific humidity data at 2-degree resolution was from ICOADS. Both wind speed and specific humidity databases have missing values in areas outside shipping routes, especially at high latitudes. Because Chiu et al. (2012) view oceanic evaporation, or sea surface latent heat flux (LHF) divided by the latent heat of vaporization (Lv), as a crucial factor of the global water and energy cycle, we used LHF data for 1950–2012 from the National Centers for Environmental Prediction/National Center for Atmospheric Research (NCEP/NCAR) Reanalysis (Kalnay et al., 1996) as a fundamental proxy for oceanic evaporation. We also used data from the Japanese Re-Analysis 55 Years (JRA-55) (Kobayashi et al., 2015) and the European Centre for Medium-Range Weather Forecasts (ECMWF) 40-year Reanalysis (ERA-40) (Uppala et al., 2005) datasets and compared these datasets to the LHF data from NCEP/NCAR and the moisture flux vector. Based on the comparison, we addressed possible reliability problems in moisture data from the pre-satellite era. Although there are some differences between these three databases, the differences do not significantly influence our conclusions. Our analysis primarily used July-August-September (JAS) averages, corresponding to the Sahel region's rainy season.

Figure 1 shows the long-term value of JAS average precipitation in northern Africa using PREC_L data. Our study area, defined as the region bounded by 10°N-20°N and 8°W-30°E, was chosen to avoid coastal influences on seasonal rainfall in the Sahel. The JAS has captured, by

120 definition, the Sahel region rainy season between 200 to 600 mm per JAS per year and we used
121 the PREC_L data for the smooth resolution of the data. Figure 2 shows the variation of JAS
122 average rainfall in the study area from 1950 through 2012. Sahel rainfall decreased from the
123 early 1960s to the mid-1980s, followed by an increasing trend for the rest of the study period.
124 The driest year of the study period was 1984 (Munemoto and Tachibana, 2012); we focused on
125 that period to divide our dataset into two different periods, the decreasing and increasing periods.
126 The mid-1980s mark a clear reversal in these multi-decadal trends. The signature of this trend
127 shift is not sensitive to the definition of the study area (results not shown). Because the data were
128 insufficient to analyze at least two cycles of multi-decadal variability, we focused on a
129 phenomenon ("the trend shift") that might indicate a phase change.

130 To assess the degree to which trends in other climatic parameters synchronized with the
131 Sahel trend shift, we divided the time series of all datasets into the subperiods 1950–1984 and
132 1985–2012. We defined the trend in each subperiod as the angle of inclination, $\tan\theta$, of the time
133 series, as calculated from the linear regression coefficient using the least squares method. We
134 defined the strength of the trend shift, $\delta\tan\theta$, as $\tan\theta_2 - \tan\theta_1$, where the subscripts 1 and 2
135 denote the subperiods before and after 1984, respectively. To confirm that the trends of the two
136 subperiods differed in sign, we added the condition $\tan\theta_1 \cdot \tan\theta_2 < 0$. We named a decreasing to
137 increasing (increasing to decreasing) trend shift as a positive (negative) trend shift, i.e., $\delta\tan\theta >$
138 0 ($\delta\tan\theta < 0$) and $\tan\theta_1 \cdot \tan\theta_2 < 0$.

139

140 **3 Results**

141 **3.1 Trend shifts of Sahel precipitation and ocean evaporation**

142 The time series of the global JAS mean LHF decreased before the mid-1980s, followed by
143 an increase (Fig. 2). Although this increase ceased after the mid-1990s, the turning point of the
144 trend shift coincided with Sahel rainfall. Global annual mean LHF also had a similar trend shift
145 to that of the JAS mean (Li et al., 2011). This synchrony suggests that, at the multi-decadal time
146 scale, the variability of Sahel rainfall may be physically linked to the transport of the moisture
147 flux from the oceans. We also investigated global mean sensible heat flux, but found no
148 significant trends during the study period.

The trend shift of LHF in the world ocean may be related to precipitation inside and outside the Sahel. The results of our investigation of this possibility are shown for both JAS and annual precipitation of PREC_L in Figure 3a and 3b, respectively. The trend shift over the Sahel is stronger for annual precipitation than for JAS precipitation. The areas where the positive trend shifts (from decreasing to increasing) in JAS precipitation are large are the Sahel, western coastal areas of South Asia, and equatorial South America (Fig. 3a).

For annual precipitation, the areas with positive trend shifts are more numerous than the areas with negative trend shifts (Fig. 3b). Positive trend shifts are particularly strong in the Sahel, western coastal areas of South Asia, and southern Chile and less strong in Korea, Japan, the Philippines, Alaska, and northern Eurasia. Negative trend shifts are seen in South America, most of the SH, most of North America, and inland Eurasia; these areas are weaker and narrower than the areas with a positive trend shift. These results indicate that a positive trend shift in precipitation occurred not only in the Sahel but elsewhere in the globe. Comparing the trend shifts of JAS precipitation of the PREC_L (Fig.3a), GPCC (Fig. 3c), and the University of Delaware (Fig.3d) datasets, similar land coverage was observed, with a correlation of 0.9; however, the University of Delaware (Fig. 3d) dataset showed a weaker signal over the same areas included in the PREC_L and GPCC datasets.

3.2 Global SST trend shift

Sahel rainfall is related to nearby SST (Lough, 1986, Bader and Latif, 2003; Chung and Ramanathan, 2006) and remote SST (Folland et al., 1986; Janicot et al., 1996; Rowell, 2003; Fontaine et al., 2011; Munemoto and Tachibana, 2012; Diatta and Fink, 2014). Although there is not visible evidence of change, it is conceivable that the SST time series has a changing phase from 1984 using the SST over the northern hemisphere (NH) and SH. As demonstrated by Munemoto and Tachibana (2012), the NH SST became lower than that of the SH SST and described an opposite trend after 1984. Figure 4 shows that areas of positive trend shift in the JAS SST over the oceans are widespread in the NH, meaning that SST decreased until 1984 and then increased. Areas of negative trend shift are mostly in the SH, particularly the eastern tropical Pacific and the South Atlantic Ocean. The obvious contrast between hemispheres

suggests that the change in JAS Sahel rainfall is somehow related to the hemispheric contrast in SST; these results are consistent with the findings of Folland et al. (1986) and Munemoto and Tachibana (2012). In addition, modeling and observational studies by Bader and Latif (2003) show that the Sahel region rainfall variability is linked with regional and global SST anomaly patterns, which include fluctuations in: the tropical Atlantic Ocean, as pointed out by Lamb (1978), Hastenrath, (1984), and Lamb and Peppler, (1992); the Pacific Ocean, as alluded by Janicot et al. (1996) and Rowell (2001); the Indian Ocean, as referred to by Palmer (1986) and Shinoda and Kawamura (1994); and the Mediterranean, as mentioned by Rowell (2003).

3.3 Trend shift of global ocean evaporation

The time change of the SST, i.e., SST trend, should be linearly related to the evaporation from the ocean provided that the ocean is treated as a slab. The time change of the evaporation, i.e., LHF trend, should thus be linearly related to the second-order differential of the SST. Here we simply compare between the two trend shifts, because the quality of the global dataset dose not resolve the second-order differential. Figure 5a and b show the JAS trend shift's geographic distribution of land water vapor flux and global ocean evaporation, as defined by LHF using NCEP and JRA-55 data, respectively. They both show a similar signs over the oceans, except at the coastline of western South America and the tropical Atlantic; one possible explanation is that the JRA-55 data are missing at least 10 years before 1984, which could capture the tropical Atlantic magnitude. When the subtropical SH Atlantic ocean is warmer (colder) than normal, greater (lesser) LHF production is observed, with a deeper surface coverage of the moisture flux transient through the western coast of the Sahel region, whereas the NCEP data show coverage transient through the eastern Sahel coast; similar results were found by Bader and Latif (2003). The NCEP and JRA-55 datasets captured a significant relation over the Sahel region, even though the JRA-55 evaporation rate increases at the western side of Sahel region and is negative in the eastern part. The relation of the tropical Pacific ocean, El Nino, and both the northern and southern Atlantic with the Sahel's rainfall variation, which was confirmed by Zhang et al. (2006), is observed in the JRA-55 data, but not the the NCEP/NCAR data.

3.4 Trend shifts of wind, humidity

Latent heat flux is determined by surface wind speed and the humidity deficit over the ocean. As displayed on Figure 6, the trend shift of JAS surface scalar wind speeds over the ocean. This shift is positive over most of the SH, particularly in the eastern Pacific Ocean. Many of these positive areas match areas with positive LHF trend shifts (Fig. 5). In the NH, the trend shift is positive over the subtropical central and eastern Pacific. Over the western subtropical North Atlantic ocean, the trend shift in the scalar wind is not in agreement with the trend shift in LHF; nevertheless, the overall similarity of Fig. 6 and Fig. 5 signifies that trend shifts in wind speed over the ocean partially account for the trend shift in LHF.

The trend shift in the JAS deficit of surface specific humidity, as determined from its saturated value at the local SST, is shown in Fig. 7. The geographic distribution of this positive trend shift is essentially global, similar to those of SST (Fig. 4) and LHF (Fig. 5) in the NH and the southern Pacific Ocean. The positive trend shift of global evaporation from the ocean is therefore also partially explained by this trend shift.

Figure 8 shows a map of the JAS moisture flux trend shift using JRA-55. On this figure we can observe anticyclonic curvature from the eastern tropical Pacific toward tropical Atlantic; eastward flux from the tropical Atlantic to the Sahel region; the flux from Indian Ocean in about 40S trough the South Atlantic Ocean is also witnessed. This flux is further connected to the tropical Atlantic Ocean. Most importantly, this figure clearly highlights the key role the South of Indian Ocean and the East of the Pacific Ocean play in Sahel rainfall variation. In addition, a weaker transport from the North Atlantic through Mediterranean Ocean entrance to Libya is also observed, however this phenomenon is blocked by the local high pressure located in the Sahara desert.

4 Discussion and conclusion

Our study demonstrates an important synchrony between Sahel rainfall and global evaporation from oceans. The key point is that the shift in the trend of JAS Sahel rainfall from decreasing to increasing (positive trend shift) occurred in the mid-1980s and coincided with shifts in global-scale SST and evaporation from the oceans (Table 1). We found that the Sahel

trend shift was synchronous with similar positive trend shifts in global oceanic evaporation (Fig. 2) and in land precipitation outside the Sahel, except in the Americas (Fig. 3). In detail, the trend shift in oceanic evaporation (as indicated by LHF) encompassed the SH and the subtropical NH, including the Pacific, Atlantic, and Indian Oceans (Fig. 5). Because increased oceanic evaporation strengthens global moisture transport toward the land, the synchronization of these trend shifts is physically plausible, and indeed the area of increased LHF exceeded the area of decreased LHF. Trend shifts also occurred in the mid-1980s in SST: the shift was negative (increase to decrease) in the SH and positive in the NH, giving rise to an interhemispheric contrast in SST (Fig. 4). The surface scalar wind over the ocean had a positive trend shift, mainly in the SH, that extended to the subtropical Pacific Ocean in the NH (Fig. 6). The humidity deficit displayed a positive trend shift in both hemispheres, particularly in the Pacific Ocean (Fig. 7). The strongest statement comes from the vector moisture flux, which clearly represents the path of the moisture flux from the eastern Pacific and South Indian Oceans through the tropical southern Atlantic to the western entrance of the Sahel region, and also the tropical northern Atlantic through northern Europe through Libya as an entrance that was, however, dissipated by the blocked high pressure in the Sahara region (Fig. 8). The eastern Pacific and South Indian Oceans are the areas where the positive trend shift of the latent heat flux is observed (Fig. 5)

From these results, we can assert that the process that connects the trend shifts of the global oceans and Sahel rainfall (Fig. 9), which is the main reason for the positive trend shift in LHF, is the positive trend shift in scalar wind, particularly in the SH, because surface wind promotes evaporation from the ocean. When SST is greater than normal, the atmosphere becomes unstable, leading to an interaction between convection and large-scale circulation that strengthens the convergence at the surface with a low wind speed at this center, generating a small amount of latent heat flux. LHF lowers the SST due to evaporative cooling, which was also suggested by Wu et al. (2009) and Zhang et al. (1994). Therefore, the negative trend shift in SH SST may be an effect of the positive trend shift in the scalar wind. Giannini et al. (2003) and Zeng (2003) demonstrated that in the SH, when the gulf is warm, the Intertropical Convergence Zone (ITCZ) shifts south away from the Sahel, reducing the African monsoon that draws moist air into the Sahel, which means that long-term changes in Sahel rainfall are induced by changes in SST in the tropical Atlantic and Pacific oceans. The opposite way is that the advection of the magnitude of the moisture flux from the oceans toward the Sahel region forces the ITCZ to shift northward

toward the Sahel region during the boreal summer. Although the linkages can be viewed as speculative and conceptual, the phenomenon could explain why both hemispheres are correlated positively, even though their SSTs are different.

In the NH, at latitudes lower than 40°N, the LHF trend shift tended to be positive, in synchrony with the positive SST trend shift. Because high SST in low latitudes generally promotes evaporation, the positive trend shift in LHF may be a consequence of the positive trend shift in SST; the positive trend shift in the humidity deficit in the NH also supports this inference. Thus, the positive SST trend shift in the NH may be linked to the positive LHF trend shift. Although the trend shift in SST is positive in the NH and negative in the SH, hemispheric differences in the role of SST may result in a global positive trend shift in LHF.

Although our study offers an explanation for these global-scale trend shifts, the reason for the outsized signature of Sahel rainfall is still problematic. In line with our viewpoint, Pomposi et al. (2015) affirmed that "understanding of how the monsoon reacts to global SSTs remains incomplete because the system can be impacted by moisture availability locally and in the region as well as tropical atmospheric stability, both of which are influenced by ocean temperatures." In the past, the influence of SST in different remote sites was emphasized (Folland et al., 1986; Czaja and Frankignoul, 2002; Dijkstra, 2006; Ting et al., 2009), including in the Atlantic Ocean (Hu and Huang, 2006; Marullo et al., 2011; Martin et al., 2014), Pacific Ocean (Rowntree, 1972; Pan and Oort, 1983; Cayan and Peterson, 1989; Wallace et al., 1989), and Indian Ocean (Clemens et al., 1991; Ashok et al., 2001, 2003; Annamalai et al., 2005). To identify how evaporation in these remote oceans drives Sahel rainfall, idealized atmospheric general circulation model studies will need to incorporate the anomalous SST patterns shown in this study. The processes underlying the trend shift of the ocean surface wind also must be identified. Additionally, it is noteworthy that the trend shift in oceanic evaporation might affect the global salinity distribution, and in turn the global thermohaline circulation. Remarkably, the SST-Sahel teleconnection seems to be stronger with the Indian Ocean (negative correlation) and Mediterranean index (positive correlation) in about 50% of the years of that era (Fontaine et al., 2011), which led us to conclude that the resemblance between global trends and trends in the Sahel makes it difficult to attribute changes in the Sahel to only a single teleconnection. Largely, the horizontal transfer of heat flux from oceans to the Sahel region through precipitation variability (or opposite) has been highlighted.

Furthermore, our experiments confirm the hypothesis that the south Indian Ocean, east Pacific Ocean, and Atlantic Ocean significantly influence not only regional climate anomalies, as Bader and Latif (2003) suggested, but also the relationship between global changes in SSTs and the Sahel region's rainfall variability, as revealed by Folland et al. (1986). The conclusion, which one can draw from these various studies, is that the Sahel constitutes the world's largest area in which this trend shift occurred. Rainfall or dry conditions in the West African Sahel region can definitely be associated with the role of the global oceans.

Acknowledgements

We thank the Ministry of Education, Culture, Sports, Science and Technology (MEXT) for the opportunity afforded by the international student scholarship program. MEXT supported this study through a Grant-in-Aid for Scientific Research on Innovative Areas (Grant Number 22106003). We extend special thanks to Kunihiko Kodera and Koji Yamazaki for insightful discussions. We also thank the editor and anonymous reviewers for their valuable comments and suggestions to improve the quality of the paper. The Grid Analysis and Display System (GrADS) and Generic Mapping Tools (GMT) were used to draw the figures.

References

Annamalai, H., Liu, P., and Xie, S. P.: Southwest Indian Ocean SST Variability Its Local Effect and Remote Influence on Asian Monsoons, J. Climate, 18, 4150–4167, doi: 10.1175/JCLI3533.1, 2005.

Ashok, K., Guan, Z., and Yamagata, T.: Impact of the Indian Ocean dipole on the relationship between the Indian Monsoon rainfall and ENSO, Geophys. Res. Lett., 28, 4499–4502, doi:10.1029/2001GL013294, 2001.

Ashok, K., Guan, Z., and Yamagata, T.: Influence of the Indian Ocean Dipole on the Australian winter rainfall, Geophys. Res. Lett., 30, 1821-1825, doi:10.1029/2003GL017926, 2003.

Bader, J. and Latif, M.: The impact of decadal-scale Indian Ocean sea surface temperature anomalies on Sahelian rainfall and the North Atlantic Oscillation, Geophys. Res. Lett., 30, 2169-2172, doi:10. 1029/ 2003GL018426, 2003.

Baines, P. G., and Folland, C. K.: Evidence for rapid global climate shift across the late 1960s, J. Climate, 20, 2721 – 2744, doi:10.1175/ JCLI4177.1, 2007.

Cayan, D. R. and Peterson, D. H.: The Influence of North Pacific Atmospheric Circulation on Streamflow in the West, in Aspects of Climate Variability in the Pacific and the Western Americas, Geophys. Monogr., No. 55, Amer. Geophys. Union, 375–397, doi:10.1029/GM055p0375, 1989.

Chen, M., Xie, P., Janowiak, J. E., and Arkin, P. A.: Global Land Precipitation: A 50-yr Monthly Analysis Based on Gauge Observations, J. Hydrometeor., 3, 249-266, 2002.

Chiu L.S, Gao S. and Shie C-L: Oceanic Evaporation: Trends and Variability, p261, 2012.

Christensen, J.H., Hewitson, B., Busuioc, A., Chen, A., Gao, X. Held, I., Jones, R., Kolli, R. K., Kwon, W.-T., Laprise, R., Rueda, V. M., Mearns, L., Menéndez, C.G., Räisänen, J., Rinke, A., Sarr, A., and Whetton, P.: Regional Climate Projections. In: Climate Change 2007: The Physical Science Basis. Contribution of Working Group I to the Fourth Assessment Report of the Intergovernmental Panel on Climate Change [Solomon, S., D. Qin, M. Manning, Z. Chen, M. Marquis, K.B. Averyt, M. Tignor and H.L. Miller (eds.)]. Cambridge University Press, Cambridge, United Kingdom and New York, NY, USA, 2007.

Chung, C. E. and Ramanathan, V.: Weakening of North Indian SST Gradients and the Monsoon Rainfall in India and the Sahel, J. Climate, 19, 2036–2045, doi:10.1175/JCLI3820.1, 2006.

Clemens, S., Prell, W., Murray, D., Shimmield, G., and Weedon, G.: Forcing mechanisms of the Indian Ocean monsoon. Nature, 353, 720-725, doi:10.1038/353720a0, 1991.

Czaja, A. and Frankignoul, C.: Observed Impact of Atlantic SST Anomalies on the North Atlantic Oscillation, J. Climate, 15, 606–623, doi:10.1029/2004JD005676, 2002.

Dai, A.: Drought under global warming: a review, WIREs Climate Change, 2, 45-65, doi:10.1002/wcc.81, 2011.

Delworth, T. L., Manabe, S., and Stouffer, R. J.: Interdecadal variations of the thermohaline circulation in a coupled ocean-atmosphere model, J. Climate, 6, 1993 – 2010, doi:10.1175/1520-0442(1993)006<1993:IVOTTC>2.0.CO;2, 1993.

353 Diatta, S. and Fink, A. H.: Statistical relationship between remote climate indices and West
354 African monsoon variability, Int. J. Climatol., 34-12, 3348-3367, doi:10.1002/joc.3912, 2014.

355 Dijkstra, H. A.: Interaction of SST Modes in the North Atlantic Ocean, J. Phys. Oceanogr., 36,
356 286–299, doi:10.1175/JPO2851.1, 2006.

357 Folland, C. K, Palmer, T. N., and Parker, D. E.: Sahel rainfall and worldwide sea temperatures,
358 1901-85, Nature, 320, 602-607, doi:10.1038/320602a0, 1986.

359 Fontaine, B., Gaetani, M., Ullmann, A., and Roucou, P.: Time evolution of observed July–
360 September sea surface temperature-Sahel climate teleconnection with removed quasi-global
361 effect (1900–2008), J. Geophys. Res., 116, D04105, doi:10.1029/2010JD014843, 2011.

362 Giannini, A., Saravanan, R., and Chang, P.: Oceanic forcing of Sahel rainfall on annually to
363 interdecadal time scales, Science, 302, 1027–1030, doi:10.1126/science.1089357, 2003.

364 Hagos, S. M. and Cook, K. H.: Ocean Warming and Late-Twentieth-Century Sahel Drought and
365 Recovery, J. Climate, 21, 3797-3814, doi:10.1175/2008JCLI2055.1, 2008.

366 Hastenrath, S.: Interannual Variability and Annual Cycle: Mechanisms of Circulation and
367 Climate in the Tropical Atlantic Sector, Mon. Weather Rev., 112, 1097-1107, doi:10.1175/1520-
368 0493(1984)112<1097:IVAACM>2.0.CO;2, 1984.

369 Hoerling, M., J. Hurrell, Eischeid, J. and Phillips, A.: Detection and attribution of 20th century
370 northern and southern African rainfall change, 19, 3989-4008, J. Climate, 2006.

371 Hu, Z. Z. and Huang, B.: Physical Processes Associated with the Tropical Atlantic SST
372 Meridional Gradient, J. Climate, 19, 5500–5518, doi:10.1175/JCLI3923.1, 2006.

373 Hulme M.: Rainfall changes in Africa: 1931–1960 to 1961–1990. Int. J. Climatol. 12: 685–699,
374 1992.

375 Janicot, S., Moron, V., and Fontaine, B.: Sahel droughts and ENSO dynamics, Geophys. Res.
376 Lett., 23, 515–518, doi:10.1029/96GL00246, 1996.

377 Kalnay E., Kanamitsu, M., Kistler, R., Collins, W., Deaven, D., Gandin, L., Iredell, M., Saha, S.,
378 White, G., Woollen, J., Zhu, Y., Cheillab, M., Ebsuzaki, W., Higgins, W., Janowiak, J., Mo, K.

C., Ropelewski, C., Wang, J., Leetma, A., Reynolds, P., Jenne, R., and Joseph, D.: The NCEP/NCAP 40-year reanalysis project, B. Am. Meteorol. Soc., 77, 437-470, 1996.

Kobayashi, S., Ota, Y., Harada, Y., Ebita, A., Moriya, M., Onoda, H., Onogi, K., Kamahori, H., Kobayashi, C., Endo, H., Miyaoka, K., and Takahashi, K.: The JRA-55 Reanalysis: General Specifications and Basic Characteristics, J. Meteorol. Soc. Jpn, 93, 5-48, doi:10.2151/jmsj.2015-001, 2015.

Lamb, P. J., and R. A. Peppler: Further Case Studies of Tropical Atlantic Surface Atmospheric and Oceanic Patterns Associated with Sub-Saharan Drought, J. Climate, 5, 476-488, doi:10.1175/1520-0442(1992)005<0476:FCSOTA>2.0.CO;2, 1992.

Lamb, P. J.: Large-scale Tropical Atlantic surface circulation patterns associated with Subsaharan weather anomalies. Tellus, 30, 240-251, 1978.

Li, G., B. Ren, J. Zheng, and C. Yang: Trend singular value decomposition analysis and its application to the global ocean surface latent heat flux and SST anomalies, J. Climate, doi:10.1175/2010JCLI3743.1, 2011.

Lough, J. M.: Tropical Atlantic Sea Surface Temperatures and Rainfall Variations in Subsaharan Africa, Mon. Weather. Rev., 114, 561–570, doi:10.1175/1520-0493(1986)114<0561:TASSTA>2.0.CO;2, 1986.

Lu, J., and T. Delworth: Oceanic forcing of the late 20th century Sahel drought. Geophys. Res. Lett., 32, L22706, doi:10.1029/2005GL023316, 2005.

Martin, E. R., Thorncroft, C., and Booth, B. B.: The Multidecadal Atlantic SST—Sahel Rainfall Teleconnection in CMIP5 Simulations, J. Climate, 27, 784–806, doi:10.1175/JCLI-D-13-00242.1, 2014.

Marullo, S., Artale, V., and Santoleri, R.: The SST Multidecadal Variability in the Atlantic–Mediterranean Region and Its Relation to AMO, J. Climate, 24, 4385–4401, doi:10.1175/2011JCLI3884.1, 2011.

Munemoto, M. and Tachibana, Y.: The recent trend of increasing precipitation in Sahel and the associated inter-hemispheric dipole of global SST, Int. J. Climatol., 32, 1346–1353, doi:10.1002/joc.2356, 2012.

Omotosho, J. B.: Pre-rainy season moisture build-up and storm precipitation delivery in the West African Sahel. Int. J. Climatol., 28 937–946, 2008.

Palmer, T. N.: Influence of the Atlantic, Pacific and Indian Oceans on Sahel rainfall, Nature, 322, 251-253, doi:10.1038/322251a0, 1986.

Pan, Y. H. and Oort, A. H.: Global Climate Variations Connected with Sea Surface Temperature Anomalies in the Eastern Equatorial Pacific Ocean for the 1958–73 Period, Mon. Weather. Rev., 111, 1244–1258, doi:10.1175/1520-0493(1983)111<1244:GCVCWS>2.0.CO;2, 1983.

Rowell, D. P.: The Impact of Mediterranean SSTs on the Sahelian Rainfall Season, J. Climate, 16, 849–862, doi:10.1175/1520-0442(2003)016<0849:TIOMSO>2.0.CO;2, 2003.

Rowell, D. P.: Teleconnections between the tropical Pacific and the Sahel. Q. J. R. Meteorol. Soc., 127, 1683–1706, 2001.

Rowntree, P. R.: The influence of tropical east Pacific Ocean temperatures on the atmosphere, Q. J. R. Meteorol. Soc., 98, 290–321, doi:10.1002/qj.49709841605, 1972.

Schneider, U., Becker, A., Finger, P., Meyer-Christoffer, A., Rudolf, B., and Ziese, M.: GPCC Full Data Reanalysis Version 6.0 at 2.5°: Monthly Land-Surface Precipitation from Rain-Gauges built on GTS-based and Historic Data, doi: 10.5676/DWD_GPCC/FD_M_V7_250, 2011.

Shinoda, M., and Kawamura, R.: Tropical rainbelt, circulation, and sea surface temperatures associated with the Sahelian rainfall trend. J. Meteor. Soc. Japan, 72, 341-357, 1994.

Smith, T. M., Reynolds, R. W., Peterson, T. C., and Lawrimore, J.: Improvements to NOAA's Historical Merged Land-Ocean Surface Temperature Analysis (1880-2006), J. Climate, 21, 2283–2296, 2008.

Stott, P. A., Gillett, N. P., Hegerl, G. C., Karoly, D. J., Stone, D. A., Zhang, X., and Zwiers, F.: Detection and attribution of climate change: A regional perspective, Wiley Interdiscip. Rev. Clim. Change, 1, 192-211, 2010.

Ting, M., Kushnir, Y., Seager, R., and Li, C.: Forced and Internal Twentieth-Century SST Trends in the North Atlantic, J. Climate, 22, 1469–1481, doi:10.1175/2008JCLI2561.1, 2009.

433 Tippett, M., and Giannini, A.: Potentially predictable components of African summer rainfall in
434 an SST-forced GCM simulation, J. Climate, 19, 3133–3144, 2006.

435 Tokinaga, H. and Xie, S. P.: Wave and Anemometer-based Sea Surface Wind (WASWind) for
436 Climate Change Analysis, J. Climate, 24, 267-285, doi:10.1175/2010JCLI3789.1, 2011.

437 Uppala and co-authors : The ERA-40 re-analysis, Q. J. R. Meteorol. Soc., 131, 2961–3012,
438 doi:10.1256/qj.04.176, 2005.

439 Wallace, J. M., Mitchell, T. P., and Deser, C.: The Influence of Sea-Surface Temperature on
440 Surface Wind in the Eastern Equatorial Pacific: Seasonal and Interannual Variability, J. Climate,
441 2, 1492–1499, doi:10.1175/1520-0442(1989)002<1492:TIOSST>2.0.CO;2, 1989.

442 Wolter, K.: Modes of tropical circulation, Southern Oscillation, and Sahel rainfall anomalies, J.
443 Climate, 2, 149-172, doi:10.1175/1520-0442(1989)002<0149:MOTCSO>2.0.CO;2, 1989.

444 Wu R., Kirtman, B. P., and Pegion, K.: Surface latent heat flux and its relationship with sea
445 surface temperature in the National Centers for Environmental Prediction Climate Forecast
446 System simulation and retrospective forecasts, Geophys. Res. Lett., 34, L17712,
447 doi:10.1029/2007GL030751, 2009.

448 Xue, Y., Smith, T. M., and Reynolds, R. W.: Interdecadal changes of 30-yr SST normals during
449 1871-2000, J. Climate, 16, 1601-1612, doi:10.1175/1520-0442-16.10.1601, 2003.

450 Zhang, R., and Delworth, T. L.: Impact of Atlantic multidecadal oscillations on India/Sahel
451 rainfall and Atlantic hurricanes, Geophys. Res. Lett., 33, L17712, doi:10.1029/2006GL026267,
452 2006.

453 Zeng, N.: Drought in the Sahel, Science, 302, 999–1000, 2003.

454 Zhang G.,J, and Mcphaden M. J.: The relationship between sea surface temperature and latent
455 heat flux in the equatorial Pacific, J. Climate, 8(3), 589–605, 1995.

456 Table 1. Summary of Results for JAS Meteorological Parameters. “Positive” indicates that a shift
457 from decrease to increase occurred during 1950 to 2012; “negative” indicates a shift from
458 increase to decrease.

459

	Sahel rain	SST	LHF	Wind	Humidity deficit
Northern hemisphere	Positive	Positive	Positive	Positive (tropical Pacific)	Positive
Southern hemisphere		Negative	Positive	Positive	Positive (Pacific)

460

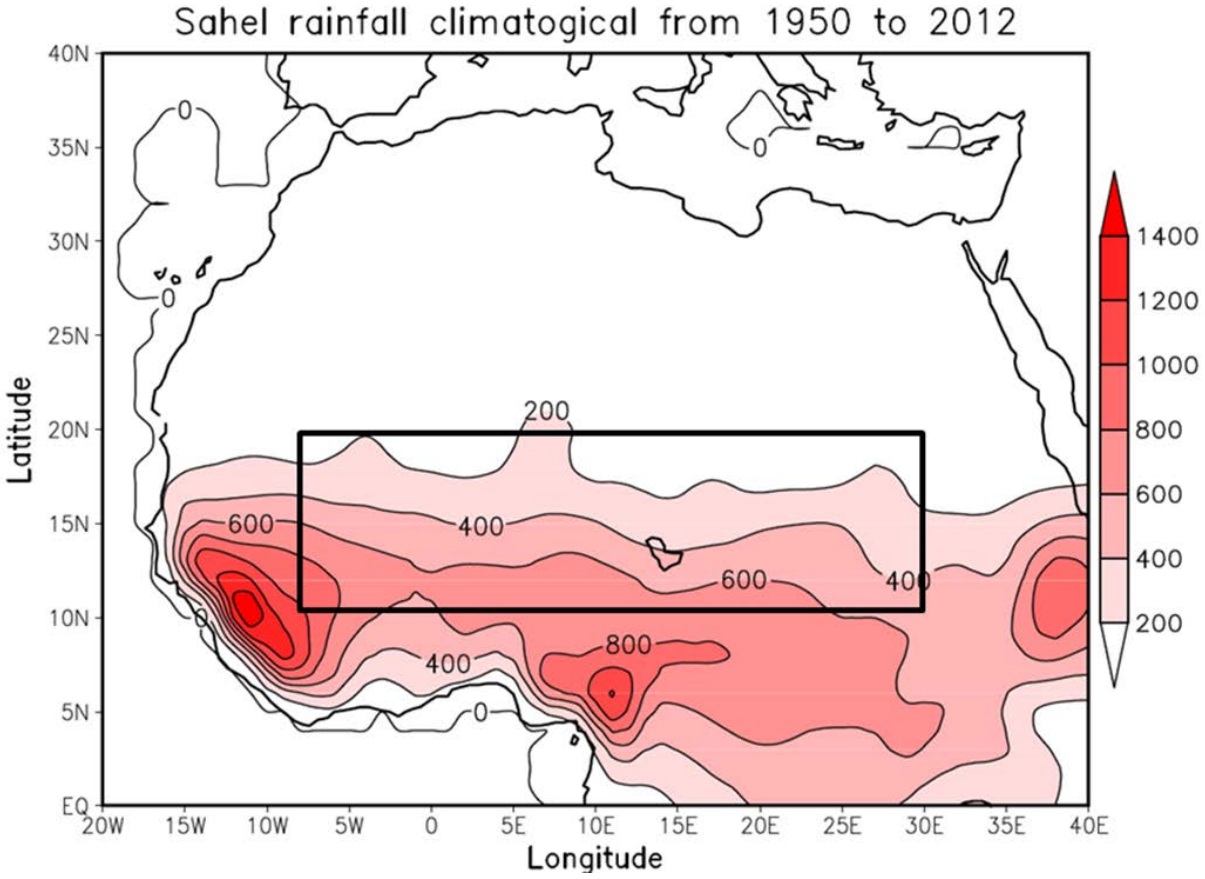

Fig.1 Climatological JAS mean of North Africa region rainfall averaged from 1950 to 2012. The area defined as the Sahel region is in the rectangle between latitude 10-20°N and longitude 8°W-30°E. The unit is mm.

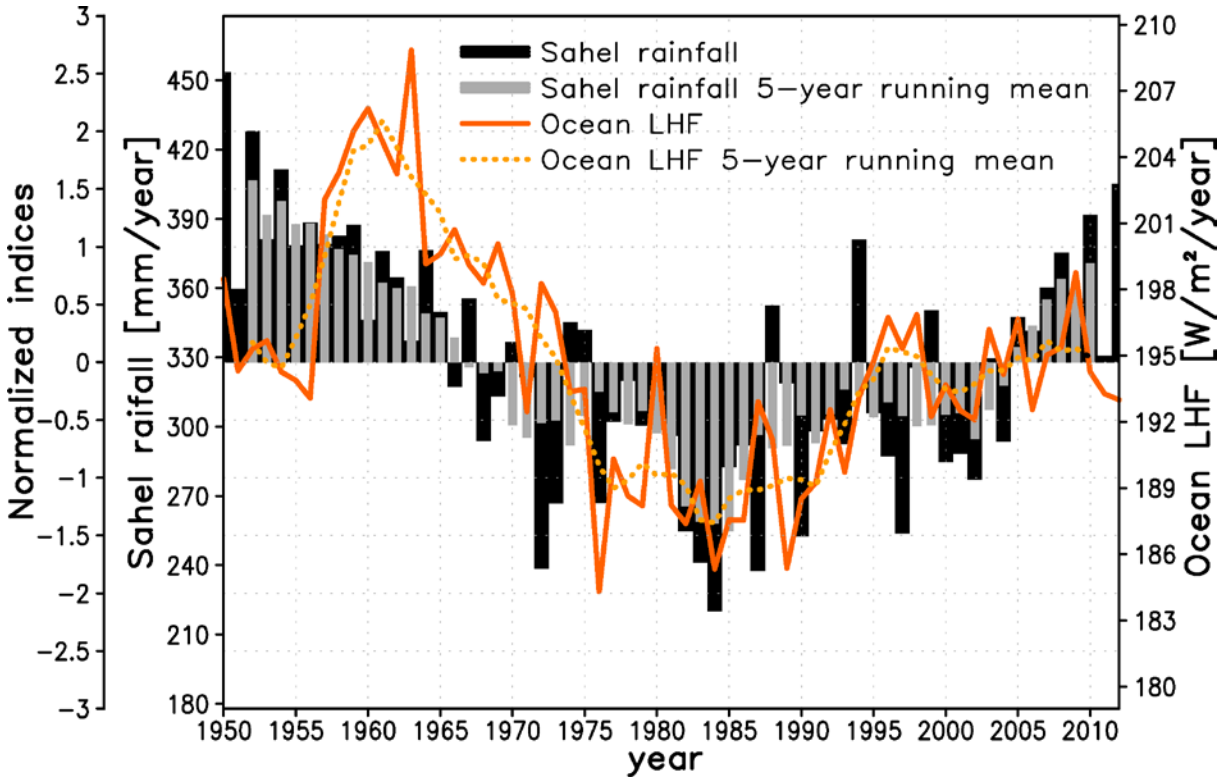

Figure 2. Time series of JAS Sahel rainfall (mm) and mean LHF ($W\ m^{-2}$) from oceans from 1950 to 2012.

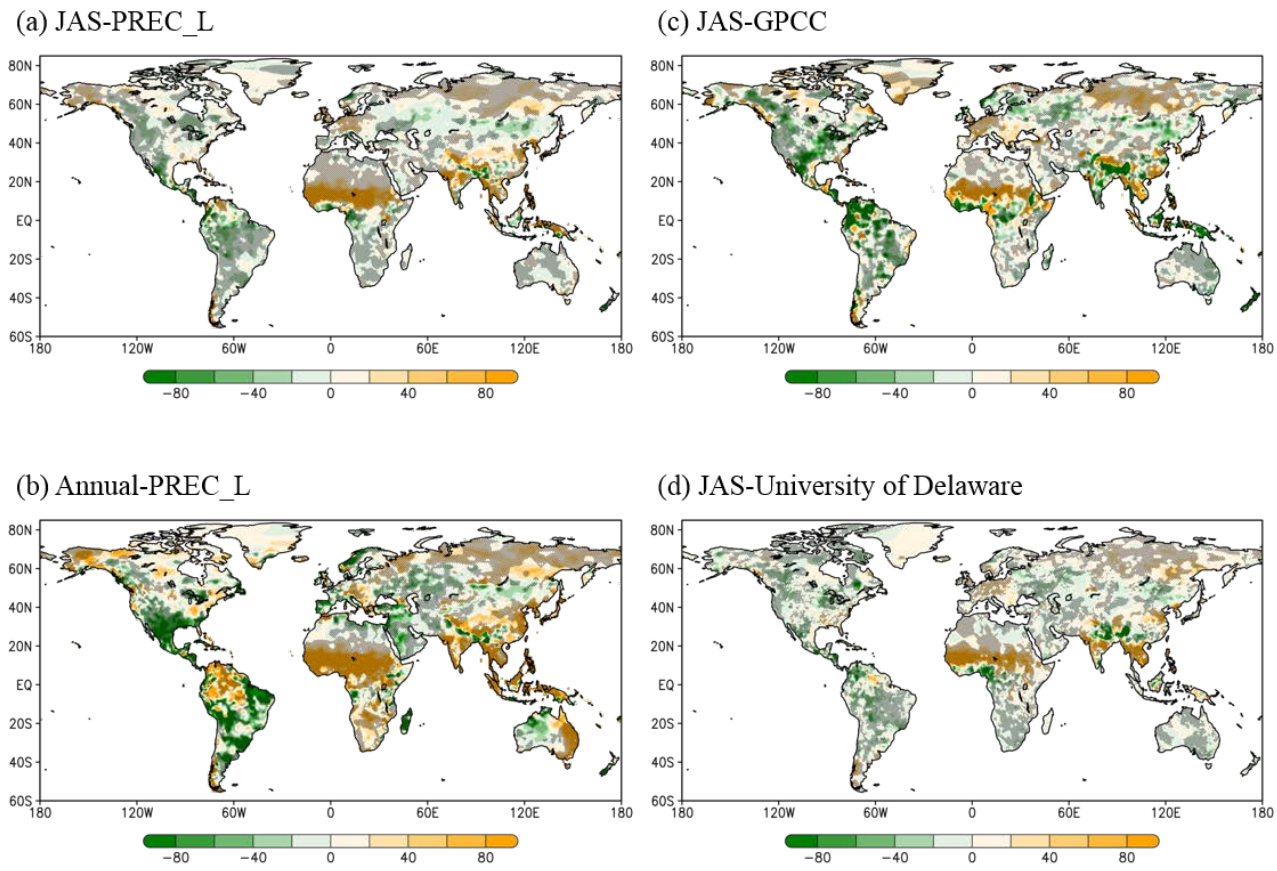

475

476 Figure 3. Global maps of the trend shift for (a) JAS precipitation PREC_L (mm 10years^{-1}), (b)
477 annual precipitation, (c) JAS precipitation GPCC and (d) JAS precipitation University of
478 Delaware. Shading denotes $\delta \tan\theta$. Hatching represents areas where trends changed sign
479 between the two parts of the study period ($\tan\theta_1 \cdot \tan\theta_2 < 0$).

480

481

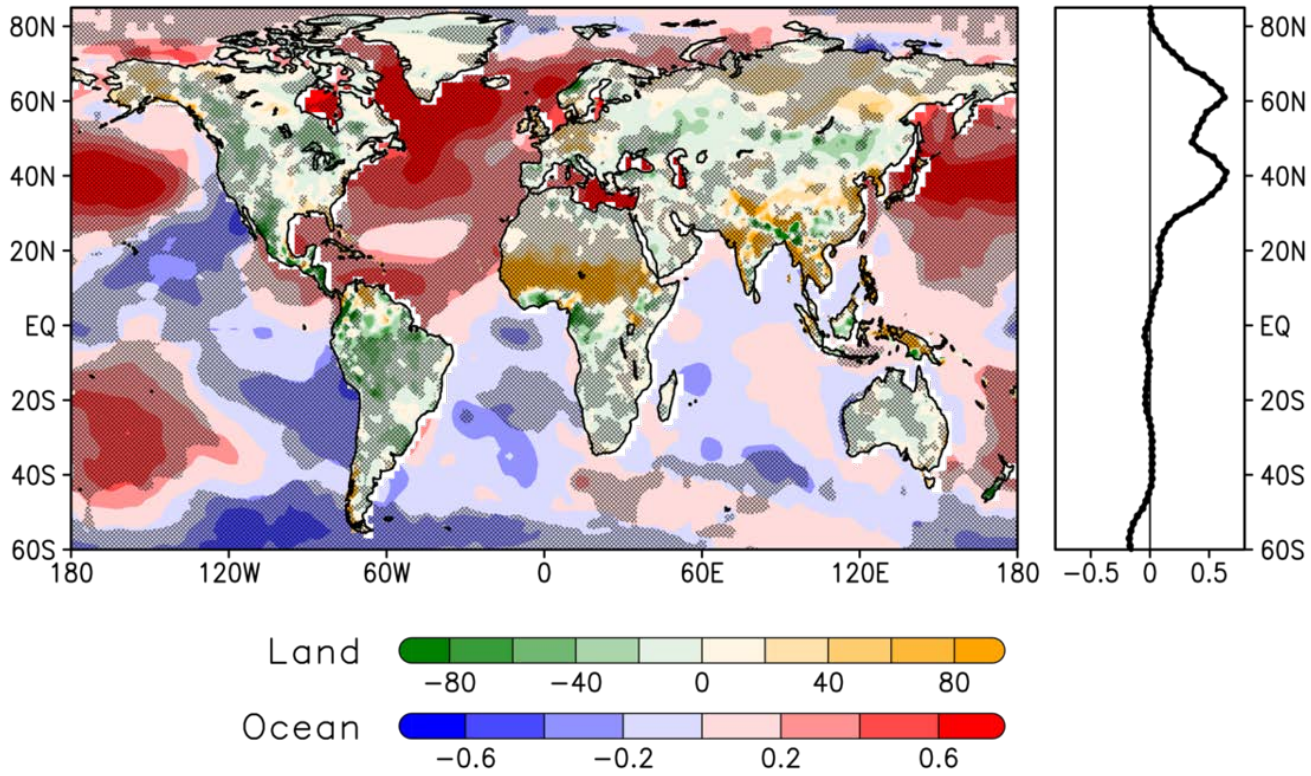

Figure 4. (Left) Trend shifts in SST (K/10years) and (Right) latitude profile of its zonal mean. Land areas display trend shifts in JAS precipitation from Fig. 3a. Hatching represents areas where trends changed sign between the two parts of the study period ($\tan\theta_1 \cdot \tan\theta_2 < 0$).

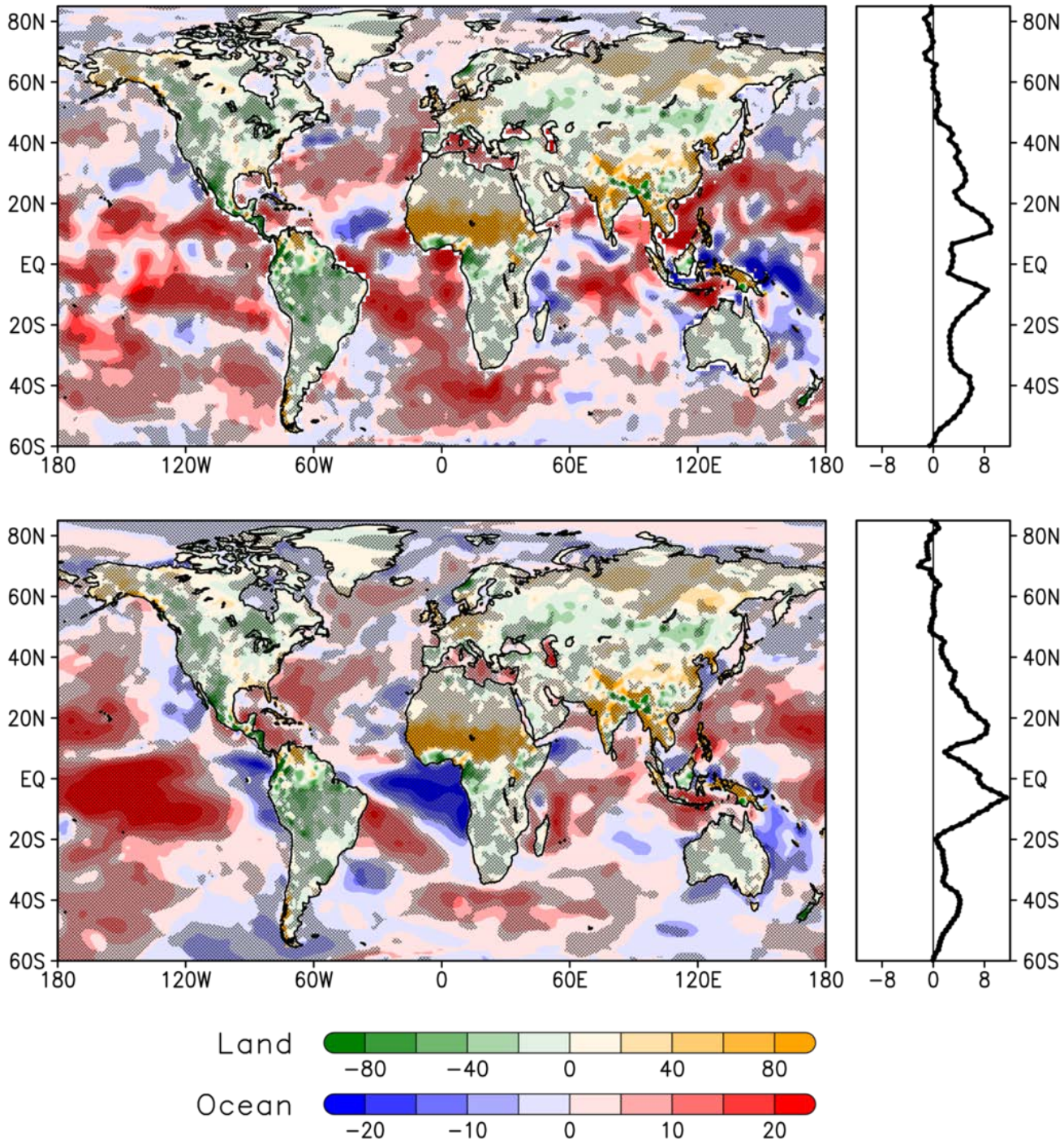

494

495 Figure 5. Global maps of the LHF trend shift over the oceans for (a) JAS-NCEP (W m^{-2}/10years) and (b)JAS-JRA55. Land areas display trend shifts in JAS precipitation from Fig. 3a.
496
497 Shading denotes $\delta \tan\theta$. Hatching represents areas where trends changed sign between the two
498 parts of the study period ($\tan\theta_1 \cdot \tan\theta_2 < 0$).

499

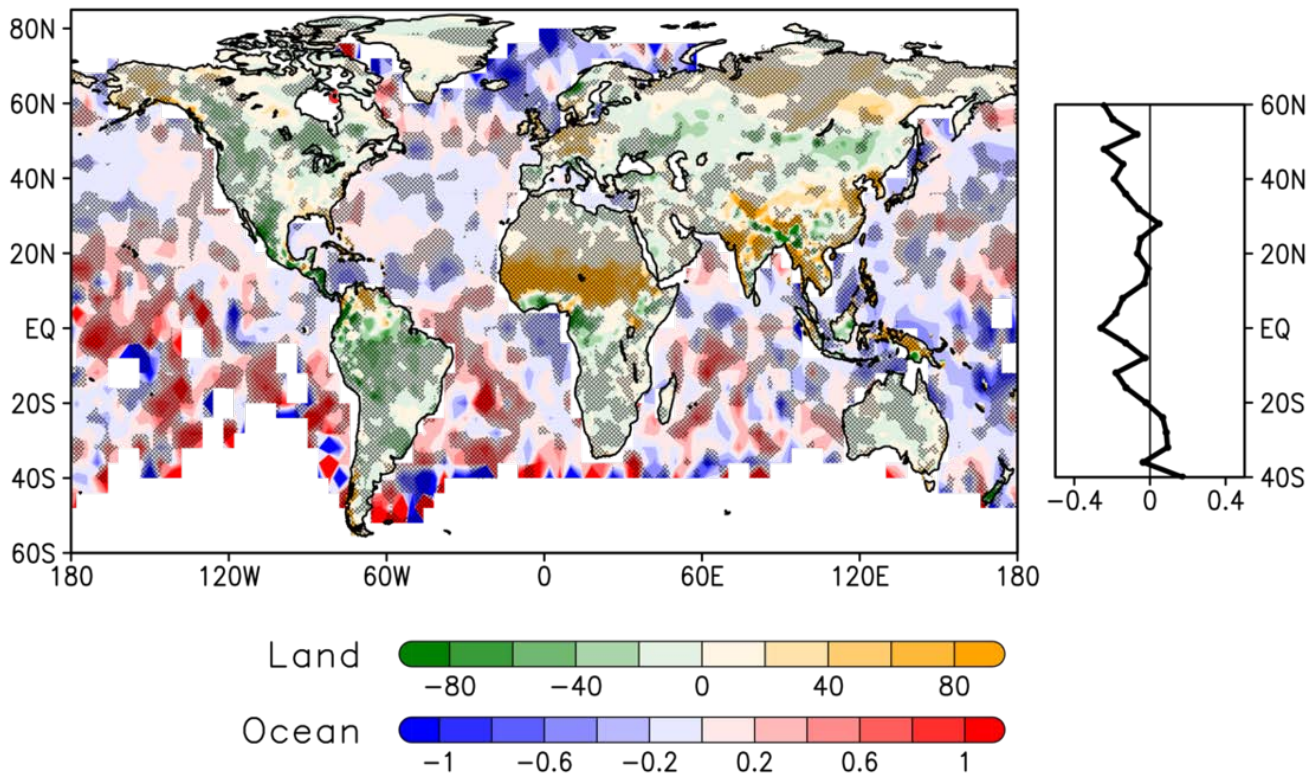

Figure 6. (Left) Trend shifts in scalar wind speed over the ocean (m s^{-1}/10years) and (Right) latitude profile of its zonal mean. Land areas display trend shifts in JAS precipitation from Fig. 3a. Hatching represents areas where trends changed sign between the two parts of the study period ($\tan\theta_1 \cdot \tan\theta_2 < 0$).

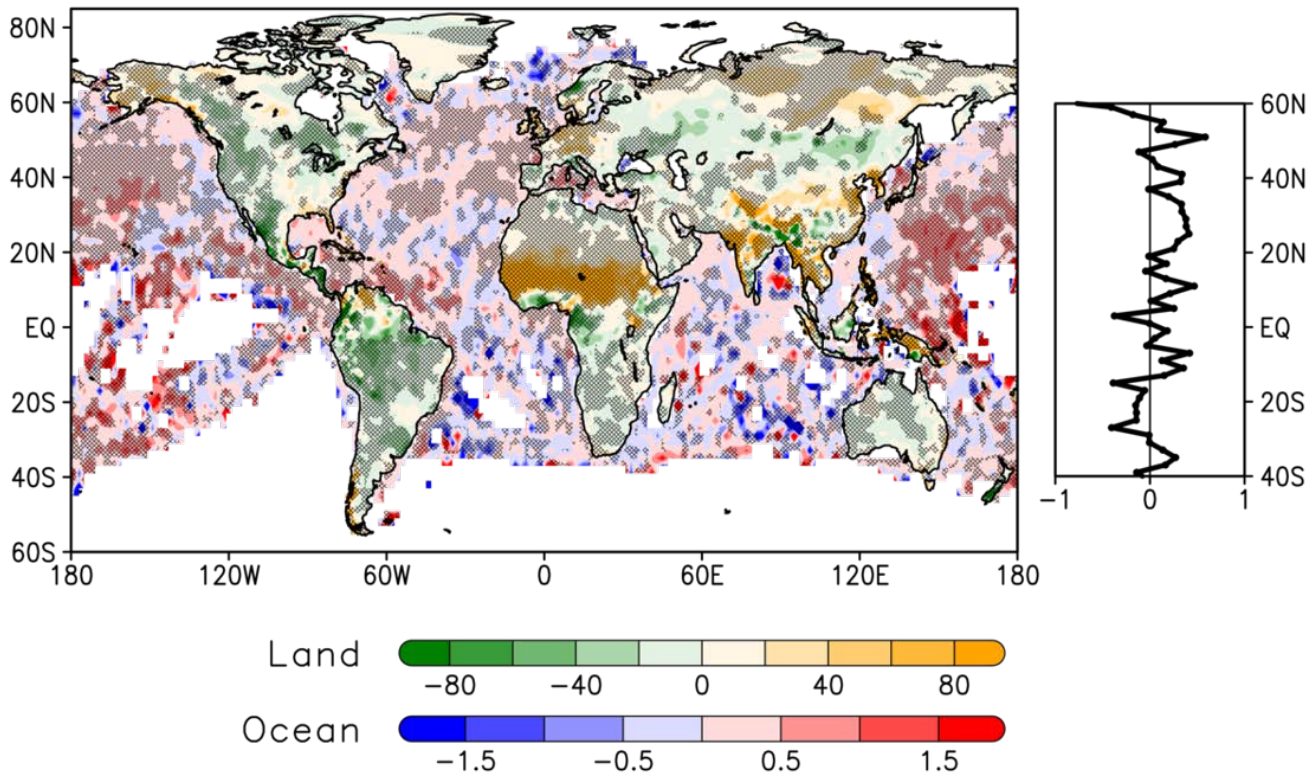

507

508

509 Figure 7. (Left) Trend shifts in the humidity deficit (g kg^{-1}/10years) over the ocean and (Right)
510 latitude profile of its zonal mean. Land areas display trend shifts in JAS precipitation from Fig.
511 3a. Hatching represents areas where trends changed sign between the two parts of the study
512 period ($\tan\theta_1 \cdot \tan\theta_2 < 0$).

513

514

515

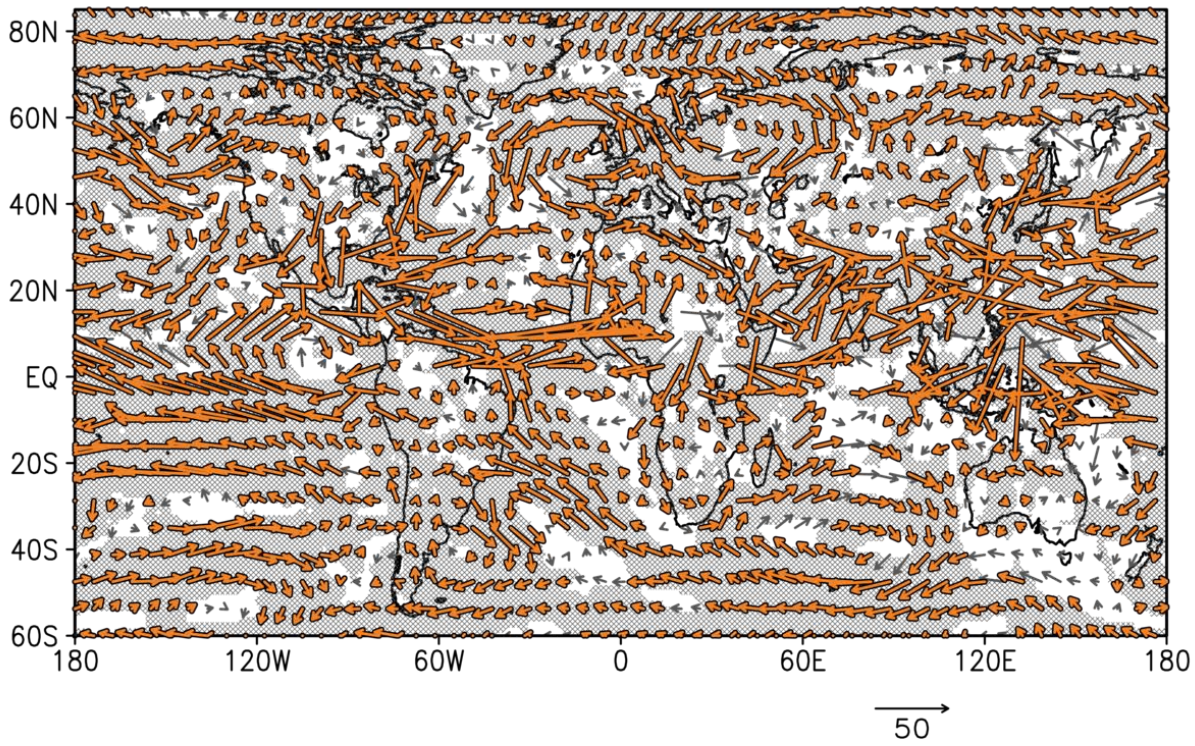

516

517 Figure 8. Trend shift vector map of moisture flux using JRA-55 (kg m^{-1} s^{-1}/10years, 1958-2014:
518 JAS). Orange bold vector and hatching represent areas where northward or eastward moisture
519 flux trends changed sign between the two parts of the study period ($\tan\theta_1 \cdot \tan\theta_2 < 0$).

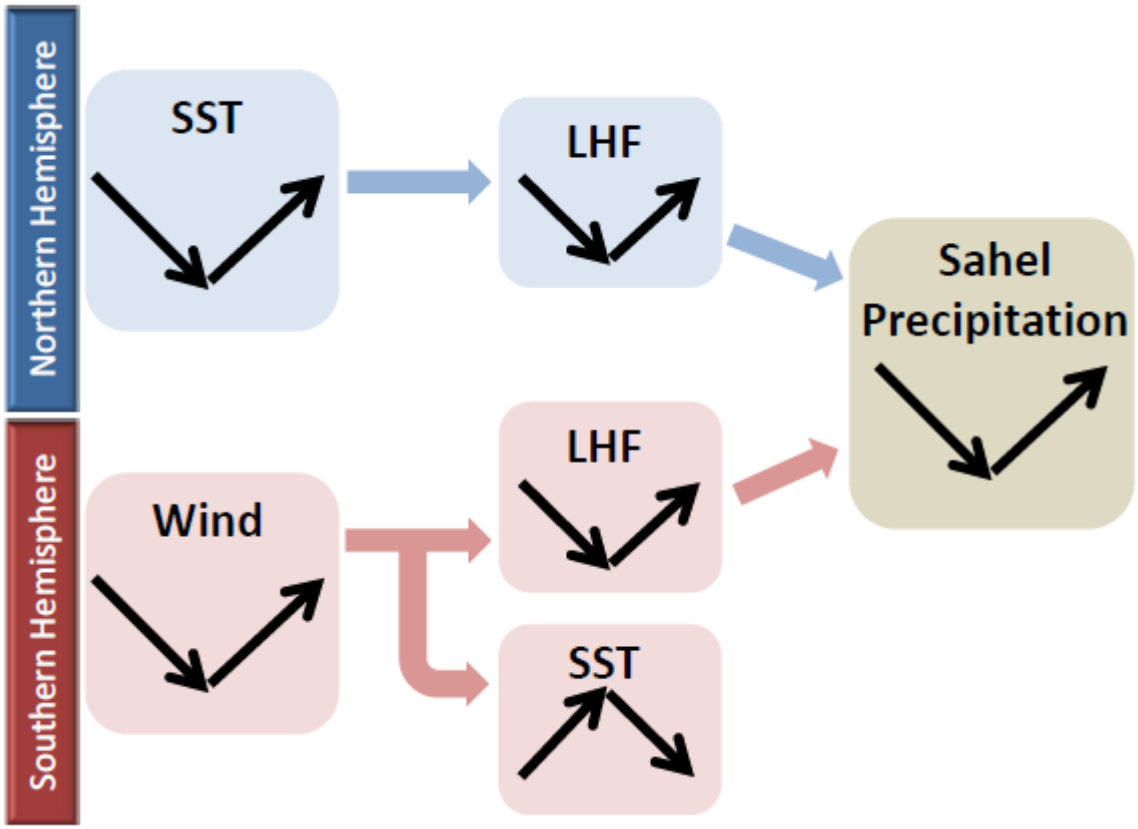

Figure 9. Schematic diagram of possible processes linking Sahel precipitation and the global ocean. The arrows represent increases or decreases in a parameter during 1950–1984 and 1985–2012.